Analytic formulation and parametrization of the kinetic potential theory for drizzle formation

Robert McGraw and Yangang Liu
Environmental Sciences Department, Atmospheric Sciences Division, Brookhaven National Laboratory, Upton, New York 11973, USA
(Received 12 February 2004; published 27 September 2004)

The kinetic potential of nucleation theory is extended to describe cloud droplet growth processes that can lead to drizzle formation. In this model drizzle formation is identified as a statistical barrier crossing phenomenon that transforms cloud droplets to much larger drizzle size with a rate dependent on turbulent diffusion, droplet collection efficiency, and properties of the underlying cloud droplet size distribution. Closed-form expressions for the kinetic potential, critical drop volume, barrier height, and both steady-state and transient barrier crossing drizzle rates are obtained in terms of measurable cloud properties. In an analogy with the theory of phase transformation, clouds are classified into two regimes: an activated metastable regime, in which there is a significant barrier and drizzle initiation resembles nucleation, and an unstable regime where kinetics dominates analogous to the spinodal regime of phase transformation. Observational evidence, including the threshold behavior of drizzle formation and the well-known effect that aerosols have on drizzle suppression, is shown to favor drizzle formation under activated conditions (more similar to nucleation than spinodal decomposition) and under transient conditions rather than steady state. These new applications of the kinetic potential theory should lead to more accurate parametrizations of aerosol-cloud interaction and improved algorithms for weather forecasting and climate prediction.

DOI: 10.1103/PhysRevE.70.031606 PACS number(s): 64.60.Qb, 05.40.−a, 92.60.Nv, 82.60.Nh

I. INTRODUCTION

Drizzle is an important cloud process that plays a crucial role in regulating the Earth's energy balance and water cycle [1]. Drizzle also affects climate through its influence on cloud lifetime and cloud cover [2]. The formation of drizzle consists of two steps: cloud formation, and the subsequent autoconversion process whereby large cloud droplets collect smaller ones and become embryonic raindrops. The first process involves heterogeneous nucleation on aerosol particles already present in the precloud environment. These particles, depending on their number concentration and wetting properties, determine the cloud droplet number concentration N_D. Meteorological conditions including temperature and concentration of water vapor also play an important role in determining number concentration through their influence on the fraction of aerosol particles that activate to become cloud droplets [3]. Meteorological conditions also determine the liquid water fraction $L = \mathrm{cm}^3(\mathrm{liquid})/\mathrm{cm}^3(\mathrm{air})$, which is the product of N_D and average cloud droplet volume.

The present study is focused on the autoconversion process, whereby large droplets form, fall through, and collect the smaller ones under warm rain conditions for which the ice phase plays no role [4,5]. Understanding and accurate parametrization of autoconversion is especially important for studies of cloud lifetime and of the so-called second aerosol indirect effect: namely, the observation that higher cloud droplet number concentrations result in suppression of rain [6,7].

The drizzle process has long been a puzzle in that the droplets would seem to take longer to form than the lifetime of a typical rain cloud. A key property of the new model is that it provides a barrier mechanism for limiting the number of very small (embryonic) drizzle drops. This reduces the subsequent competition for cloud water and thus the time required for measurable drizzle formation. Drizzle formation is identified as a statistical barrier crossing phenomenon that transforms cloud droplets to drizzle size with a rate dependent on turbulent diffusion, droplet collection efficiency, and properties of the size distribution.

To develop the present drizzle model we adapt methods traditionally used in homogeneous nucleation theory even though autoconversion is not usually thought of as a nucleation process. Closed-form expressions for the barrier profile, height, and critical droplet size are derived in Sec. II. The steady-state rate of barrier crossing is obtained in Sec. III. The approach used here follows the Becker-Döring-type multistate kinetics calculations of homogeneous nucleation rate but the underlying physics is different. In particular the droplet surface tension, which is crucial to nucleation, plays no explicit role in drizzle formation. A scaling theory is developed and a universal, closed-form expression for the steady-state barrier crossing rate is obtained in terms of two nondimensional variable groups that characterize properties of the cloud. Transient effects are analyzed in Sec. IV using a matrix approach borrowed from time-dependent nucleation theory and modified here to handle a subsampled lattice of discrete droplet sizes. We conclude with evidence that in most cases drizzle formation occurs under activated cloud conditions (i.e., with a significant barrier to the formation of large drops present) and under transient conditions rather than steady state.

II. KINETIC POTENTIAL THEORY OF DRIZZLE FORMATION

Consider a water droplet containing g molecules interacting and exchanging material with its surrounding vapor. Its kinetic potential [8] is defined as

 ©2004 The American Physical Society

$$\Phi(g) = -\ln\left(\prod_{i=1}^{g-1}\frac{\beta_i}{\gamma_{i+1}}\right) = -\sum_{i=1}^{g-1}\ln\left(\frac{\beta_i}{\gamma_{i+1}}\right), \tag{2.1}$$

where $\beta_i(s^{-1})$ is the rate of monomer addition to a drop containing i molecules and γ_i is the corresponding evaporation rate. These fluxes are correlated with the equilibrium population of drops of size g, $n_g(\mathrm{cm}^{-3})$, through the detailed balance condition.

$$\beta_g n_g = \gamma_{g+1} n_{g+1}. \tag{2.2}$$

Combining Eqs. (2.1) and (2.2) gives $n_{g+1}/n_g = \beta_g/\gamma_{g+1} = \exp\{-[\Phi(g+1)-\Phi(g)]\}$ and thus a Boltzmann-type proportionality for the equilibrium population: $n_g \propto \exp[-\Phi(g)]$. These considerations support the idea that Eq. (2.1) defines a "potential," albeit one that is defined solely in terms of kinetic coefficients. In nucleation theory, n_g is identified with the constrained equilibrium cluster population [9,10] and the kinetic potential is equivalent to the reduced thermodynamic potential $W(g)/kT$, where T is temperature, k is the Boltzmann constant, and $W(g)$ is the reversible work required to assemble a cluster of size g from the parent phase. Nevertheless, the kinetic potential, defined solely in terms of rate constants, is more general and can be applied even in the absence of a well-defined temperature, thermodynamic potential, or equilibrium condition.

To apply the kinetic potential to drizzle formation, the growth of cloud droplets is modeled as a sum of contributions from condensation and collection processes

$$\beta_g = \beta_g^{\mathrm{cond}} + \beta_g^{\mathrm{coll}} \tag{2.3}$$

together with an effective evaporation rate γ_g^{eff}. Collection refers to the volumetric gain of a specified drop large enough to have a significant gravitational fall velocity so as to accrete the smaller, slower falling droplets, that typify the main population of the cloud. Collection is thus an additional growth mechanism that, following the axiom "the rich get richer," becomes available to those relatively few droplets that through chance fluctuations reach fall velocity size. For collector drops of radius less than 50 μm the volumetric gain is approximated as [11]

$$\frac{dv}{dt} = \kappa v^2 L, \tag{2.4}$$

where v is the volume of the collector droplet, $\kappa = 1.1 \times 10^{10}\ \mathrm{cm}^{-3}\mathrm{s}^{-1}$, and L is the cloud liquid water volume fraction. In molecular units

$$\beta_g^{\mathrm{coll}} = \frac{dg}{dt} = \frac{1}{v_1}\frac{dv}{dt} = \kappa v_1 g^2 L, \tag{2.5}$$

where v_1 is the volume per molecule in the liquid water phase.

The condensation rate includes effects due to turbulence fluctuations that in turn cause fluctuations in the local supersaturation in the cloud. If S denotes the saturation ratio (equal to unity for a drop in equilibrium with its vapor) then fluctuations in S will cause random sustained periods of droplet growth or evaporation depending on whether S exceeds or is less than unity. This is depicted schematically in Fig. 1. In addition to turbulence fluctuations there are complicated interactions between droplets in a cloud due, for example, to the competition for available water vapor. To include such processes, we introduce an effective evaporation rate γ_g^{eff} determined from β_g^{cond} so as to yield a specified cloud droplet distribution through detailed balance. The collection term [Eq. (2.5)] applies to the much fewer number of large drops and is assumed to have negligible effect on the background cloud droplet distribution.

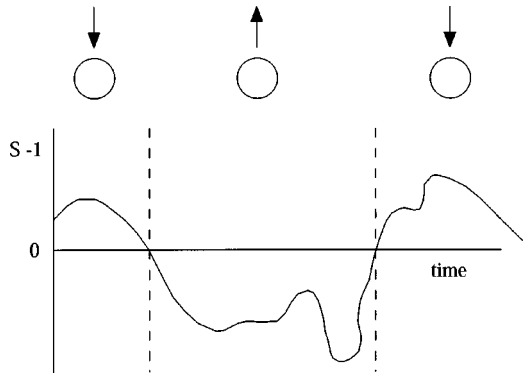

FIG. 1. Schematic depiction of droplet evaporation and growth process in a turbulent cloud. Droplet growth (represented by the downward arrows) occurs at times when the local saturation ratio S exceeds unity. When S is less than unity evaporation of the droplet occurs. Such fluctuations in S can result in Brownian-like fluctuations in droplet size.

As in our initial study [5] we assume an exponential cloud droplet distribution

$$n_g^0 = \frac{N_D}{a}\exp(-g/a). \tag{2.6}$$

N_D is the number of droplets per unit volume and $a = L/(v_1 N_D) = \overline{v}/v_1$, where $\overline{v}$ is the mean droplet volume, controls the falloff of the distribution. The superscript refers to the distribution of the typical-size cloud droplets in the absence of collection. Substitution into the detailed balance condition [Eq. (2.2)] gives

$$\frac{n_{g+1}^0}{n_g^0} = \frac{\beta_g^{\mathrm{cond}}}{\gamma_{g+1}^{\mathrm{eff}}} = \exp(-1/a). \tag{2.7}$$

Although it is possible to carry a size dependence in β^{cond} through the calculations to follow, we will assume for the present study that this quantity is independent of size: $\beta^{\mathrm{cond}}(g) = \beta^{\mathrm{cond}}$. The second equality of Eq. (2.7) gives

$$\gamma^{\mathrm{eff}} = \beta^{\mathrm{cond}}\exp(1/a) \tag{2.8}$$

showing that for this assumed droplet distribution γ^{eff} is also independent of size. In general the effective evaporation rate γ_g^{eff} is determined from β_g^{cond} and the cloud droplet distribution by the first equality of Eq. (2.7), and β_g^{coll} is determined using a model collection kernel such as the Long kernel used to obtain Eq. (2.5). Thus the turbulent condensation rate remains as the sole adjustable parameter in the model. Equations (2.5) and (2.8), together with an estimate for β^{cond},

suffice to define all of the stepwise rate coefficients needed to complete the present drizzle model.

There is an interesting analogy between the physics underlying γ^{eff}, chosen here to satisfy detailed balance while yielding a specified population of droplets, and the early physics behind the "spontaneous emission probability" used by Einstein in his derivation of the Planck radiation law [12]. In that derivation the spontaneous emission rate was obtained by the same arguments used here—detailed balance and a Boltzmann population—long before details of the quantum theory of radiation, which permits a direct calculation of this quantity, were understood.

The shape of the kinetic potential barrier can be obtained as follows: Each increment of g corresponds to the addition of one molecule—a very small step size on the scale of cloud droplets. Accordingly, the derivative of the potential, following Eqs. (2.1) and (2.3), is to excellent approximation

$$\frac{d\Phi(g)}{dg} \approx -\ln\left(\frac{\beta_g}{\gamma_{g+1}}\right) = -\ln\left(\frac{\beta^{\text{cond}} + \beta_g^{\text{coll}}}{\gamma^{\text{eff}}}\right). \quad (2.9a)$$

Defining

$$\frac{\beta_g^{\text{coll}}}{\beta^{\text{cond}}} = \frac{\kappa v_1 L}{\beta^{\text{cond}}} g^2 \equiv cg^2$$

the quantity in parenthesis becomes

$$\frac{\beta^{\text{cond}} + \beta_g^{\text{coll}}}{\gamma^{\text{eff}}} = (1 + cg^2)\exp(-1/a).$$

Because the term cg^2 is always much less than unity, the logarithm in Eq. (2.9a) can be approximated to obtain

$$\frac{d\Phi(g)}{dg} = -\ln\left(\frac{\beta^{\text{cond}} + \beta_g^{\text{coll}}}{\gamma^{\text{eff}}}\right) = \frac{1}{a} - \ln(1 + cg^2) \approx \frac{1}{a} - cg^2. \quad (2.9b)$$

Integration of this last result gives the kinetic potential

$$\Phi(g) = \frac{g}{a} - \frac{1}{3}cg^3, \quad (2.10a)$$

where the constant of integration has been chosen such that the potential vanishes at $g=0$.

On substitution for the previously defined parameter groupings a and c, Eq. (2.10a) describes a barrier having a maximum height at the critical droplet size

$$(g^*)^2 = \frac{\beta^{\text{cond}} N_D}{\kappa L^2}, \quad (2.11a)$$

which satisfies the flux balance condition $\beta^{\text{cond}} + \beta_{g^*}^{\text{coll}} = \gamma^{\text{eff}}$. The barrier height is

$$\Phi^* = \Phi(g^*) = \frac{2}{3}\frac{g^* v_1}{\overline{v}}. \quad (2.12a)$$

The lead term on the right-hand side of Eq. (2.10a), $\Phi^0(g) = g/a$, gives the kinetic potential without collection and a Boltzmann population

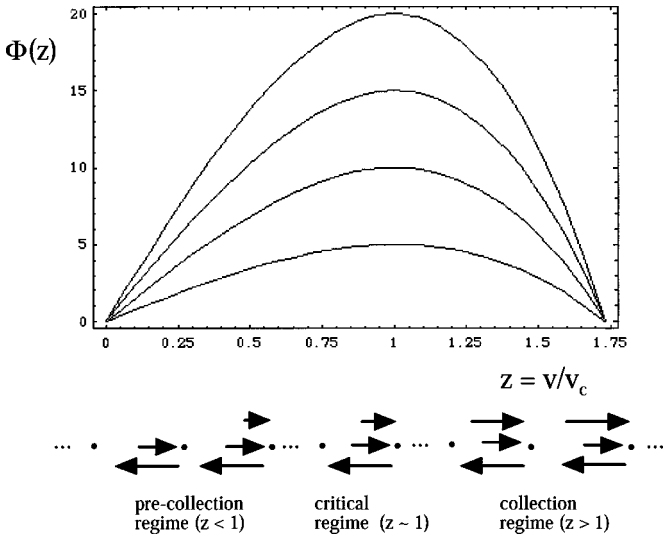

FIG. 2. Top: Kinetic potential barrier profiles from Eq. (2.10b) for several different barrier heights. Droplet size is given in reduced units where v_c is the critical droplet volume. Bottom: Schematic depiction of fluxes for condensation (middle row of arrows), evaporation (lower row of arrows), and collection (upper row of arrows). The forward and reverse fluxes are balanced at the critical droplet size. Drizzle formation requires barrier crossing, which can only occur due to fluctuations in droplet size.

$$n_g^0 \propto \exp[-\Phi^0(g)].$$

in agreement with Eq. (2.6). Its clear that in the absence of collection the critical droplet size and barrier height are infinite and drizzle cannot occur.

For applications to atmospheric physics the kinetic potential is more conveniently described in terms of the bulk parameters that characterize the cloud. These include the critical drop volume $v_c \equiv v_1 g^*$ [Eq. (2.11a)]:

$$v_c^2 = \frac{\beta^{\text{cond}} v_1^2 N_D}{\kappa L^2} \quad (2.11b)$$

and barrier height

$$\Phi^* = \frac{2}{3}\frac{v_c}{\overline{v}}. \quad (2.12b)$$

The full potential takes the form

$$\Phi(z) = \frac{\Phi^*}{2}(3z - z^3), \quad (2.10b)$$

where $z = g/g^* = v/v_c$ is the ratio of drop volume to the critical drop volume. Figure 2 (top) shows the kinetic potential at several different barrier heights according to Eq. (2.10b). The bottom panel of Fig. 2 shows a schematic depiction of the fluxes for condensation, collection, and evaporation. In the precritical droplet regime the reverse flux (evaporation) exceeds the sum of the forward fluxes due to condensation and collection and the barrier can only be surmounted due to favorable fluctuations in droplet size. This flux dominance is reversed in the postcritical, or collection, regime (i.e., the

forward fluxes dominate) with the result that growth is favored in this regime.

It is instructive to compare Eq. (2.10b) with the reduced thermodynamic barrier profile of classical nucleation theory (CNT). There $\Phi_{\mathrm{CNT}}(z)=\Phi^{*}_{\mathrm{CNT}}(3z^{2/3}-2z)$, where $z=g/g^{*}_{\mathrm{CNT}}$ is the ratio of the cluster size to the critical cluster size of the classical theory [8,13]. Indicative of fundamental differences in the underlying physics, the scaled kinetic potential for drizzle has a distinctly different shape (sharper and less rounded near the maximum) than the barrier of classical nucleation theory.

The remaining molecular grouping $\beta^{\mathrm{cond}}v_1^2(\mathrm{cm}^6\,\mathrm{s}^{-1})$, appearing in Eq. (2.11b), has an important physical interpretation: Molecular number diffusion along the g coordinate is given by the diffusion coefficient [14,13]

$$D_g=\frac{1}{2}nl^2\approx\beta^{\mathrm{cond}}, \tag{2.13}$$

where n is the total jump frequency (forward and backward jumps included) and l is the jump distance (equal to unity for single-molecular jumps). The last equality loses the factor of $1/2$ due to the fact that β^{cond} gives the frequency of only the forward jumps. By analogy we see that $\beta^{\mathrm{cond}}v_1^2$ is the (turbulent) diffusion coefficient along the *volume* coordinate—with jump size v_1. On the larger scale of cloud droplet volumes it is natural to represent processes using a subsampled lattice of droplet sizes with renormalized transition rates between adjacent sizes defined so that physical quantities such as the diffusion constant are invariant to the lattice spacing [5]. For, example, for a lattice spacing v_{step}, where $v_1\ll v_{\mathrm{step}}\ll v_c$ and rescaled coordinate $d=v/v_{\mathrm{step}}$, we obtain step-invariant diffusion along the volume coordinate

$$D_v=\beta_d^{\mathrm{cond}}v_{\mathrm{step}}^2=\beta^{\mathrm{cond}}v_1^2 \tag{2.14a}$$

provided

$$\beta_d^{\mathrm{cond}}=\beta^{\mathrm{cond}}(v_1^2/v_{\mathrm{step}}^2) \tag{2.14b}$$

is used for the (renormalized) turbulent condensation rate. This subsampled lattice plays an essential role in the transient drizzle rate calculations of Sec. IV.

A typical range for the unknown model parameter D_v, which depends on β^{cond} (also unknown), can be estimated as follows: Consider the time $t_{1\%}$ it takes to add through Brownian-like diffusion along the volume coordinate, a sufficient volume $\Delta v\approx 127\ \mu\mathrm{m}^3$, to bring about a 1% change in a typical cloud drop radius from 10 to 10.1 μm. The mean square displacement due to diffusion along the volume coordinate is $\sigma_v^2=2D_vt$ after a time t. Equating σ_v and Δv gives

$$t_{1\%}=\frac{(\Delta v)^2}{2D_v}. \tag{2.15a}$$

Equivalently, D_v could be set in a seemingly less arbitrary way by considering the time it takes for droplets to gain or lose volumes comparable to the average cloud droplet volume

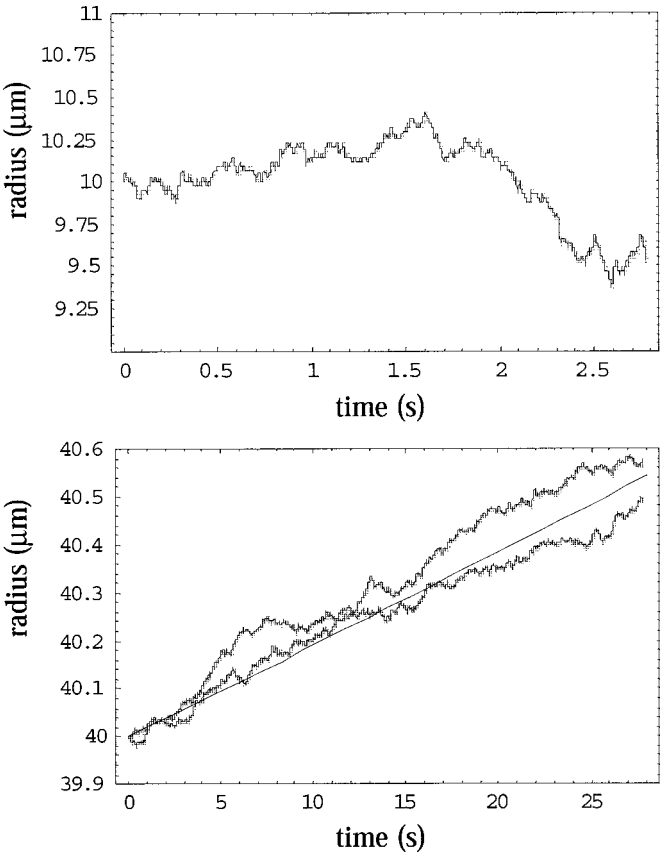

FIG. 3. Monte Carlo simulation of Brownian fluctuations in the radius of a specified droplet for $t_{1\%}=0.1$ s, $L=0.5\ \mathrm{cm}^3\ \mathrm{m}^{-3}$, $N_d=100$. (a) Precollection regime, initial droplet radius=10 μm; (b) collection regime, initial droplet radius=40 μm. The deterministic (fluctuations averaged out) growth curve in the collection regime is from Eq. (A10a) and (A10b).

$$t_v^{-}=\frac{L^2}{2D_vN_D^2}, \tag{2.15b}$$

which is a measure of the overall relaxation time of the cloud droplet distribution. The disadvantages of setting D_v using Eq. (2.15b) are its dependencies on both L and N_D and the fact that a full turbulence simulation over the considerably longer time scale t_v^{-}will be much more difficult to carry out for comparison with the present Brownian model. Following McGraw and Liu [5], we estimate D_v (or β^{cond}) through the assignment of a reasonable range of values to $t_{1\%}$:

$$D_v(\mu\mathrm{m}^6\ \mathrm{s}^{-1})\approx 8.94\times 10^{-22}\beta^{\mathrm{cond}}\approx 8.05\times 10^3/t_{1\%}(\mathrm{s}). \tag{2.16}$$

We will generally choose values of $t_{1\%}$ in the range 0.1–10 s. Longer times would not allow for significant fluctuations in drop size over the lifetime of a typical cloud and shorter times would imply growth rates faster than are likely to occur under the typical range of supersaturation found in clouds. Figure 3(a) shows a Monte Carlo simulation of Brownian fluctuations in droplet radius for $t_{1\%}=0.1$ s and a typical cloud particle size in the precollection regime. The method of simulation has been described previously in the

context of nucleation clusters [13] and cloud droplets [5]. Figure 3(b) shows the results of two different simulations beginning with an initial particle radius of 40 μm in the collection regime. Here fluctuations are evident even in the presence of net steady growth from drift motion in the downward sloping part of the kinetic potential in the collection regime. The solid curve is the result of the deterministic (fluctuations averaged out) calculation of the growth rate described in Appendix A.

III. STEADY-STATE BARRIER CROSSING RATE

The present derivation of the steady-state drizzle rate follows closely the Becker-Döring molecular kinetics approach of classical nucleation theory [9] with important differences due to boundary conditions, barrier profile, and scale. It is again convenient to begin with the molecular-level description, reporting final results in terms of relevant parameters on the cloud physics scale.

Let f_g denote the population of clusters (droplets) of size g. The net flux for conversion from g to $g+1$ is

$$J_{g,g+1} = \beta_g f_g - \gamma_{g+1} f_{g+1} = \beta_g n_g \left(\frac{f_g}{n_g} - \frac{f_{g+1}}{n_{g+1}} \right), \tag{3.1}$$

where the last equality follows Eq. (2.2). The steady-state current (J_{ss}) is constant along the growth sequence and summation of Eqs. (3.1) gives

$$J_{ss} \left(\sum_{g=g\min}^{g\max} \frac{1}{\beta_g n_g} \right) = \frac{f_{g\min}}{n_{g\min}} - \frac{f_{g\max}}{n_{g\max}}. \tag{3.2}$$

In nucleation theory the ratios on the right-hand-side in $g_{\min}$ and $g_{\max}$ are set to unity and zero, respectively, as "monomer" and Szilard boundary conditions. The summation on the left is dominated by clusters near the critical size (where n_g assumes its smallest values) with the result that the computed flux is not terribly sensitive to the placement of the boundaries provided $g_{\min} \ll g^* \ll g_{\max}$ so as to include a wide range of terms about the critical size. In the drizzle model we set $g_{\min}$ in the range of the smallest cloud droplet size ($1 \ll g_{\min} \ll \overline{v}/v_1$). In this limit Eq. (2.6) reduces to

$$n_{g\min} \approx \frac{N_D}{a} = \frac{v_1 N_D^2}{L} \tag{3.3}$$

and for the lower boundary $f_{g\min}/n_{g\min} = 1$. This boundary condition is assumed to hold even with collection: Small droplets are, of course, consumed during the collection process, just as monomer is consumed during nucleation and this can prevent the occurrence of a stable steady state [15]. However, similar to nucleation theory, the present drizzle model is limited to the *onset* regime and depletion effects are beyond its scope. Candidate approaches to future treatments of the later stages of drizzle formation are briefly discussed in Sec. V.

A natural placement for the Szilard boundary condition $f_{g\max}/n_{g\max} = 0$, is to set $g_{\max} = \sqrt{3} g^*$. This size is sufficiently beyond g^* and at the zero potential crossing [see Eq. (2.10b)]: $\Phi(g_{\max}) = 0$. With these boundary conditions in place, the right-hand-side of Eq. (3.2) is unity yielding for the steady-state crossing rate

$$J_{ss} = \left(\sum_{g=g\min}^{g\max} \frac{1}{\beta_g n_g} \right)^{-1} = \frac{v_1 N_D^2}{L} \left(\sum_{g=g\min}^{g\max} \frac{1}{\beta_g \exp[-\Phi(g)]} \right)^{-1}. \tag{3.4}$$

In the last equality the condition $\Phi(g_{\min}) \approx 0$ has been used. The β_g appearing in Eq. (3.4) is the total forward growth rate, which as already noted is dominated by the condensation rate. This is true even for clusters many times critical size. Thus we can neglect the collection term in the kinetic prefactor [it is of course included in $\Phi(g)$] and make the excellent approximation

$$\beta_g \approx \beta^{\mathrm{cond}}. \tag{3.5}$$

This and replacement of the discrete sum by an integration simplifies the final result

$$\begin{aligned} J_{ss} &= \frac{\beta^{\mathrm{cond}} v_1 N_D^2}{L} \left(\int_{g_{\min}}^{g_{\max}} \exp[\Phi(g)] dg \right)^{-1} \\ &= \kappa L v_c N_D \left(\int_0^{\sqrt{3}} \exp[\Phi(z)] dz \right)^{-1}. \end{aligned} \tag{3.6}$$

To obtain the last equality, substitute for the critical drop volume using Eq. (2.11b) and use the integration limits $z_{\min} = g_{\min}/g^* \approx 0$ and $z_{\max} = g_{\max}/g^* = \sqrt{3}$.

The integral of Eq. (3.6) is now approximated using the method of steepest descent [9]. First, expand the potential in a Taylor series about its maximum

$$\Phi(z) = \Phi^* - \frac{3}{2}\Phi^* (z-1)^2 + O\{(z-1)^3\}. \tag{3.7}$$

Substitution into Eq. (3.6) retaining through the quadratic term gives a Gaussian integral that is readily evaluated in closed form. The result is

$$\left(\int_{-\infty}^{\infty} \exp[\Phi_G(z)] dz \right)^{-1} \approx \sqrt{\frac{3\Phi^*}{2\pi}} \exp(-\Phi^*), \tag{3.8}$$

where the subscripted kinetic potential denotes the Gaussian approximation. Provided the integrand is sharply peaked near the critical size, the limits of integration can be replaced by $z_{\min}$ and $z_{\max}$, as in Eq. (3.6), with insignificant error. The final result for the barrier crossing rate ($\mathrm{cm}^{-3}\,\mathrm{s}^{-1}$) is

$$J_{ss} \approx \kappa L v_c N_D \sqrt{\frac{3\Phi^*}{2\pi}} \exp(-\Phi^*) = \beta^{\mathrm{cond}} n_{g_{\min}} Z \exp(-\Phi^*). \tag{3.9}$$

In classical nucleation theory a term similar to

$$Z = \frac{1}{g^*} \sqrt{\frac{3\Phi^*}{2\pi}} \tag{3.10}$$

is known as the Zeldovich factor [9] and corrects for barrier recrossing. Not surprisingly, its precise form in nucleation theory differs from the result obtained here.

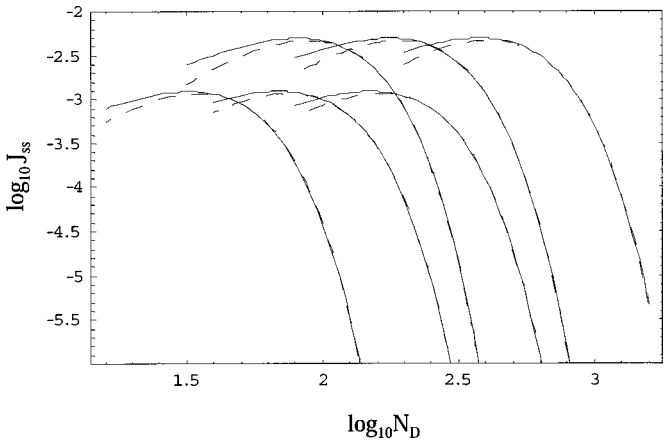

FIG. 4. Steady state barrier transmission rate (cm^{-3} s^{-1}). Results are for cloud liquid water contents of $L=0.5$ cm^3 m^{-3} (three lower pairs of curves) and $L=1.0$ cm^3 m^{-3} (three upper pairs of curves). In each set of curves for fixed L, the values of $t_{1\%}$, increasing from left to right, are 0.1, 1.0, and 10 s. The dashed curves are from Eq. (3.9). The corresponding solid curves give the exact results from numerical integration of Eq. (3.6).

Equation (3.9) provides a convenient analytic expression that is in excellent agreement with the full Becker-Döring integration of Eq. (3.6) for the steady-state drizzle rate in the activated cloud regime (see below). Figure 4 shows rates predicted from Eq. (3.9) as a function of droplet concentration for different values of L and $t_{1\%}$. Associated with each dashed curve from Eq. (3.9) is a solid curve showing the corresponding result obtained from numerical integration of Eq. (3.6) without the Gaussian approximation. Each family of curves has identical shape on the log-log scale and can be compressed to a single universal curve in appropriately scaled units. The relevant dimensionless groups are

$$\varepsilon \equiv \frac{D_v N_D^3}{\kappa L^4} = \left(\frac{v_c}{\bar{v}}\right)^2 \tag{3.11a}$$

with D_v in cgs units, and

$$\omega \equiv \frac{J_{ss}}{\kappa L^2} \tag{3.11b}$$

in terms of which Eq. (3.9) takes the universal form

$$\omega = \frac{1}{\sqrt{\pi}}\varepsilon^{3/4}\exp\left(-\frac{2}{3}\varepsilon^{1/2}\right). \tag{3.12}$$

Figure 5 (top panel) shows the universal curves from Eq. (3.12) (dashed curve) and from numerical integration of Eq. (3.6) (solid curve). That the latter is also scalable follows because the integral depends only on reduced barrier height. The bottom panel shows the reduced barrier height as a function of the logarithm of ε.

Conditions at the maximum value of the scaled drizzle rate $\{\varepsilon=(3/2)^4, \Phi^*=3/2\}$ separate the kinetically controlled and activated drizzle formation regimes. Returning to the top panel of Fig. 5 it is seen that the discrepancy between Eq. (3.12) and the exact integration appears as one enters the kinetic regime. This is due to failure of the Gaussian approximation used in the derivation of Eq. (3.9) (the integrand is no longer sharply peaked near the critical size). On the other hand, the figures show the approximation working very well in the activated regime. Figure 6 shows a number of properties predicted by the model for $t_{1\%}=0.1$ s. The solid contours are curves of constant nucleation rate obtained from the full integration of Eq. (3.6) so as to accurately describe conditions in the kinetic regime. Dashed contour lines are lines of constant radius determined from the average cloud droplet volume $\bar{v}=L/N_D$. The thick line marks the separation boundary, at $\varepsilon=(3/2)^4$, between the kinetic and activated regimes. Above this boundary (in the kinetic regime) the rate is seen to depend only on drop number, increasing as N_D is increased and, unlike the situation below the boundary, there is no sharp threshold effect.

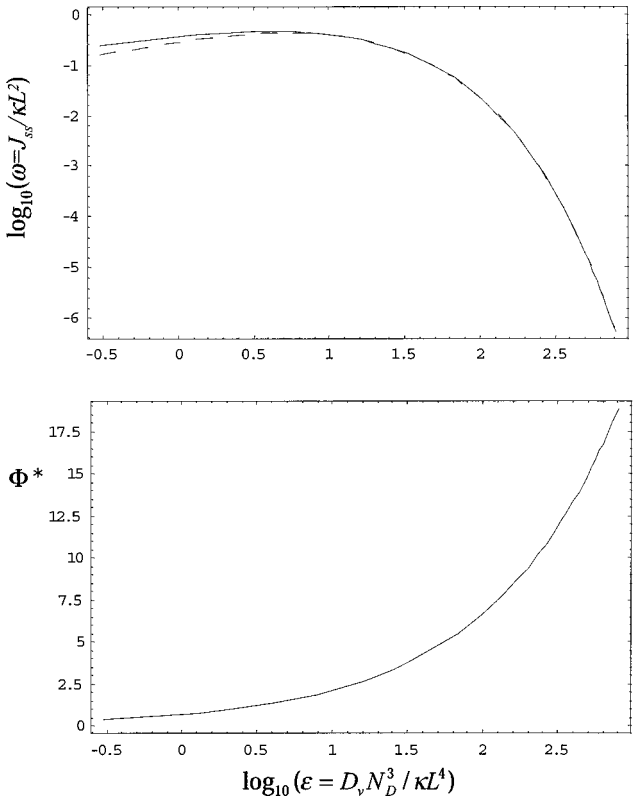

FIG. 5. (a) Universal curves for the steady-state barrier crossing rate in dimensionless coordinates (ε,ω) defined in terms of cloud properties by Eq. (3.11a) and (3.11b). Dashed curve is the analytic result from Eq. (3.12), solid curve is the exact result from numerical integration of Eq. (3.6). (b) Barrier height vs ε.

The activated and kinetic regimes of clouds (Fig. 6) are qualitatively analogous to the nucleation and spinodal regimes of phase separation. In the spinodal regime, phase separation is activationless and kinetics dominates. Strictly speaking the nucleation barrier vanishes at a true spinodal as the system passes from a thermodynamically stable state to an unstable one [16]. Classical nucleation theory has the weakness that the barrier does not vanish at the spinodal unless refinements to the theory are made [17]. The KP drizzle model also gives a nonvanishing barrier along the separation boundary $\Phi^*=3/2$, but because the analogy is only qualitative this is not necessarily a weakness in the

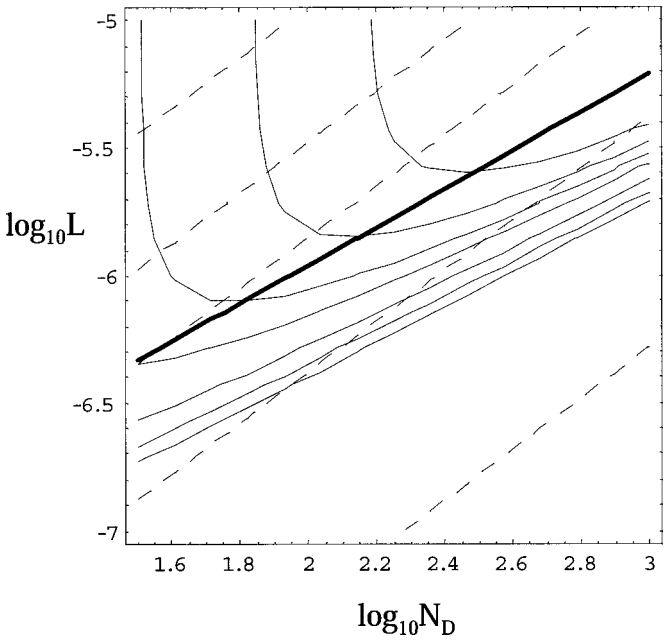

FIG. 6. Contours of constant steady state barrier crossing rate, J_{SS} cm^{-3} s^{-1}. Solid curves bottom to top: $\{\log_{10} J_{SS}=-6,-5,-4,-3,-2.5,-2,-1.5\}$. Results are from numerical integration of Eq. (3.6). Dashed lines, contours of constant mean droplet radius in micrometers, values bottom to top: $\{r=5,10,15,20,30\ \mu\text{m}\}$. Thick line, separation boundary between the kinetic and activated cloud regimes $\{\varepsilon=(3/2)^4\}$. Results are for $t_{1\%}=0.1$ s. The close contour spacing in the activated regime is indicative of threshold behavior.

theory. In practice, the distinction between $3/2$ and zero is inconsequential as such small values for Φ^* would correspond, in a true thermodynamic system, to a barrier height of only $3/2kT$ (Appendix A). Under these conditions fluctuations will dominate with the result that neither barrier height nor critical droplet volume play significant roles in the kinetic regime. Another difference from CNT is that droplet models of phase separation cannot be used within the spinodal region, whereas the KP theory continues to apply both within and outside of the kinetic regime to yield definite predictions for drizzle rate (Fig. 6).

At larger values of ε, the drizzle rate is controlled mainly by the barrier height. In this activated regime the cloud can be thought of as metastable (as opposed to unstable) and the analogy between drizzle formation and nucleation most applies. Here increases in droplet concentration result in higher barriers and sharp, thresholdlike *reductions* in drizzle rate. This behavior, opposite to the trend found in the kinetic regime, is consistent with the well-known effect that aerosols, which increase cloud droplet concentration, have on drizzle suppression [7,2]. This behavior is also consistent with the Kessler-type parametrizations of the autoconversion process [4,18], which prescribe both a critical radius, as an empirical constant, and a threshold condition such that there is no autoconversion when a characteristic radius is less than the prescribed critical radius. The kinetic potential theory provides an analytic expression [Eq. (2.11b)] for predicting the critical radius in autoconversion parametrizations [19]. These considerations point to observational evidence as well as to empirical model support for drizzle formation in the activated cloud regime.

IV. TRANSIENT DRIZZLE FORMATION

The matrix formulation of Shugart and Reiss, developed to describe transient effects in nucleation [20], is a powerful and elegant kinetic approach that can also applied to the problem of transient drizzle formation. Here we give a more complete description of the method than was possible in Ref. [5]. Several modifications to the original formulation including scaling and sampling of the size coordinate, and renormalization of the corresponding growth/evaporation rates, are introduced to extend the method from the molecular cluster scale of nucleation to the macroscopic scale of clouds and drizzle drop formation.

A. Matrix formulation

The effectively continuous population of droplet sizes is first discretized along the volume coordinate in order that the rate matrix, whose dimension will equal the number of sampled droplet sizes or lattice grid points $d=0,1,2,\ldots,G$, where $d=v/v_{\text{step}}$ in the case of equal spacing, be of manageable size. Truncating as before at $v_{\max}=\sqrt{3}v_c$ gives $v_{\text{step}}=\sqrt{3}v_c/G$. The cloud droplet distribution is also defined on the lattice. From Eq. (2.6)

$$n_d^0=\frac{v_{\text{step}}N_D^2}{L}\exp[-\Phi^0(d)], \tag{4.1}$$

where Φ^0 is the kinetic potential in the absence of collection, as defined in Sec. II, and the shortened notation $\Phi^0(d)\equiv\Phi^0(dv_{\text{step}})$ is used. In the limit of a very fine grid, $N_D=\Sigma_{d=0}^{G}n_d^0$. For coarser grids the normalization is improved using half-integer values of $d:d\rightarrow d+1/2$ in the equations below. Evolution of the drop population f_d follows the correspondingly subsampled version of Eq. (3.1):

$$\frac{df_d}{dt}=J_{d-1,d}-J_{d,d+1}=\beta_{v_{\text{step}}}f_{d-1}-\left(\beta_{v_{\text{step}}}+\beta_{v_{\text{step}}}\frac{n_{d-1}}{n_d}\right)f_d + \beta_{v_{\text{step}}}\frac{n_d}{n_{d+1}}f_{d+1}, \tag{4.2a}$$

where $\beta_{v_{\text{step}}}\equiv\beta^{\text{cond}}(v_1^2/v_{\text{step}}^2)$ is the renormalized condensation rate from Eq. (2.14b). For a constant step size this is also constant. For the smallest droplets the boundary condition $f_0/n_0=1$ gives

$$J_{0,1}=\beta_{v_{\text{step}}}n_0\left(1-\frac{f_1}{n_1}\right) \tag{4.2b}$$

where the constrained smallest cluster population n_0 is approximated using $n_0\approx n_0^0$ from Eq. (4.1).

Equations (4.2a) and (4.2b) are conveniently collected in matrix-vector form

$$\frac{d\mathbf{f}}{dt}=\mathbf{K}\cdot\mathbf{f}+\mathbf{a}, \tag{4.3}$$

with $\mathbf{f}^{\mathbf{T}}=[f_1,f_2,\ldots,f_{G-1},f_G]$, where $\mathbf{f}^{\mathbf{T}}$ denotes the transpose of $\mathbf{f}$. The growth sequence is terminated by placing the

Szilard boundary at $G+1: f_{G+1}/n_{G+1}=0$. The vector **a** accounts for the small-drop boundary condition [Eq. (4.2b)]. Its only nonzero element is $a_1=\beta_{v_{\text{step}}} n_0 \approx \beta_{v_{\text{step}}} n_0^0$. Elements of the tridiagonal matrix **K** follow inspection of Eqs. (4.2a) and (4.2b):

$$K_{d,d-1} = \beta_{v_{\text{step}}},$$

$$K_{d,d} = -\beta_{v_{\text{step}}} - \beta_{v_{\text{step}}}(n_{d-1}/n_d),$$

$$K_{d,d+1} = \beta_{v_{\text{step}}}(n_d/n_{d+1}). \tag{4.4}$$

To obtain the steady-state droplet population let

$$\mathbf{f} = \mathbf{g}_{\mathbf{SS}} + \mathbf{g}_T \tag{4.5}$$

where $\mathbf{g}_{\mathbf{SS}}$ and $\mathbf{g}_T$ are the steady state and transient components, respectively, of **f**. Substitution into Eq. (4.3) gives

$$\frac{d\mathbf{g}_T}{dt} = \mathbf{a} + \mathbf{K}\cdot\mathbf{g}_{\mathbf{SS}} + \mathbf{K}\cdot\mathbf{g}_T. \tag{4.6}$$

The requirement that the transient solution vanish at long time implies $\mathbf{a}+\mathbf{K}\cdot\mathbf{g}_{\mathbf{SS}}=0$, yielding the steady-state droplet population through matrix inversion

$$\mathbf{g}_{\mathbf{SS}} = -\mathbf{K}^{-1}\cdot\mathbf{a}. \tag{4.7}$$

As there is no return flux from drops of size $d=G+1$, due to the boundary condition, the steady-state drizzle rate is simply equal to the forward flux

$$J_{\text{SS}} = \beta_{v_{\text{step}}}(\mathbf{g}_{\mathbf{SS}})_G \tag{4.8}$$

where $(\mathbf{g}_{\text{SS}})_G = f_G(\infty)$ is the last component of $\vec{g}_{\text{SS}}$, which equals the last component of **f** at $t=\infty$. The rate from Eq. (4.8) is equivalent to the Becker-Döring result [Eq. (3.2)], but with summation here over the coarser lattice grid.

The combination of Eqs. (4.6) and (4.7) yields an equation for the transient solution

$$\frac{d\mathbf{g}_T}{dt} = \mathbf{K}\cdot\mathbf{g}_T. \tag{4.9}$$

The standard approach to solving Eq. (4.9) [20,21] involves first bringing **K** to Hermitian form. Inspection of Eqs. (4.4) for the elements of **K** reveals that although this matrix is nonsymmetric, its off-diagonal elements are related through detailed balance. Rewriting the nucleation current $J_{d,d+1}$ gives

$$J_{d,d+1} = K_{d+1,d} f_d - K_{d,d+1} f_{d+1},$$

which, under conditions of constrained equilibrium ($J_{d,d+1}=0$) gives the detailed balance condition

$$K_{d+1,d} = K_{d,d+1}(n_{d+1}/n_d) = K_{d,d+1}\exp[\Phi(d) - \Phi(d+1)], \tag{4.10}$$

where the shortened notation $\Phi(d) \equiv \Phi(dv_{\text{step}})$ is used. Equation (4.10) provides the basis for transforming **K** to Hermitian form. The square of the matrix of transformation **D** is diagonal with elements

$$D_{d,d} = \exp[\Phi(d)/kT]. \tag{4.11}$$

To demonstrate Hermiticity, consider the following matrix product

$$\mathbf{H} = -\mathbf{D}^{1/2}\mathbf{K}\cdot\mathbf{D}^{-1/2}, \tag{4.12}$$

where $\mathbf{D}^{1/2}$ is the square root of **D** and the minus sign is used to give positive eigenvalues for **H**. Similar to **K**, **H** is tridiagonal with real elements. For $\mathbf{H}^{\mathbf{T}}$, the transpose of **H**,

$$\begin{aligned}\mathbf{H}^{\mathbf{T}} &= -(\mathbf{D}^{1/2}\cdot\mathbf{K}\cdot\mathbf{D}^{-1/2})^{\mathbf{T}}\\ &= -\mathbf{D}^{-1/2}\cdot\mathbf{K}^{T}\cdot\mathbf{D}^{1/2}\\ &= -\mathbf{D}^{-1/2}\cdot\mathbf{D}\cdot\mathbf{K}\cdot\mathbf{D}^{-1}\cdot\mathbf{D}^{1/2}\\ &= -\mathbf{D}^{1/2}\cdot\mathbf{K}\cdot\mathbf{D}^{-1/2}\\ &= \mathbf{H}\end{aligned}$$

showing that **H** is Hermitian. The third equality uses the detailed balance condition in the form

$$\mathbf{K}^{\mathbf{T}} = \mathbf{D}\cdot\mathbf{K}\cdot\mathbf{D}^{-1} \tag{4.13}$$

which follows Eqs. (4.10) and (4.11).

In the frame of the transformed matrix **H**, Eq. (4.9) becomes

$$\frac{d\psi_{\mathbf{T}}}{dt} = -\mathbf{H}\psi_T, \tag{4.14}$$

where

$$\psi_T = \mathbf{D}^{1/2}\cdot\mathbf{g}_T. \tag{4.15}$$

The formal solution to Eq. (4.14) is

$$\psi_{\mathbf{T}}(t) = \mathbf{V}\,\exp(-\mathbf{D}_\lambda t)\mathbf{V}^{-1}\psi_{\mathbf{T}}(0), \tag{4.16}$$

where **V** diagonalizes **H** (specifically, the columns of **V** are comprised of the eigenvectors of **H**):

$$\mathbf{V}^{-1}\mathbf{H}\cdot\mathbf{V} = \mathbf{D}_\lambda. \tag{4.17}$$

$\mathbf{D}_\lambda$ is the diagonal matrix having the corresponding eigenvalues of **H** as elements

$$(\mathbf{D}_\lambda)_{ii} = \lambda_i.$$

With these definitions, Eq. (4.16) can be put into more explicit form. In Dirac notation

$$|\psi_{\mathbf{T}}(t)\rangle = \sum_i \langle \mathbf{V}_i|\psi_{\mathbf{T}}(0)\rangle \exp(-\lambda_i t)|\mathbf{V}_i\rangle \tag{4.18}$$

showing the dependence of the transient solution on the eigenvalues and eigenvectors of **H**. The transient droplet distribution is recovered from $\psi_{\mathbf{T}}(t)$ using Eqs. (4.5) and (4.15):

$$\vec{f}(t) = \vec{g}_{\mathbf{SS}} + \mathbf{D}^{-1/2}|\psi_{\mathbf{T}}(t)\rangle. \tag{4.19}$$

Finally, because there is no contribution to the net flux from evaporation of drops of size $d=G+1$, the transient drizzle rate, defined here as the flux to the Szilard boundary is

$$J(t) = \beta_{v_{\text{step}}} f_G(t)$$
$$= J_{\text{SS}} + \beta_{v_{\text{step}}} \mathbf{D}^{-1/2}(G,G) \sum_j \langle \psi(0) | V_j \rangle \exp(-\lambda_j t)(V_j)_G, \tag{4.20}$$

where $\mathbf{D}^{-1/2}(G,G) = \sqrt{n_G}$ and $(V_j)_G$ is the last component of eigenvector $|V_j\rangle$.

B. Calculations

To most efficiently implement Eq. (4.20) it is useful to employ the scaled z coordinate in terms of which the barrier again depends on only a single parameter ε or barrier height ($\Phi^* = 2\sqrt{\varepsilon}/3$). This enables the transient drizzle rates to be mapped to a one-parameter family of curves characterized by ε.

For the calculations that follow we set v_{step} such the number of sampled droplets G (equal to the dimensionality **H**) is 100: $v_{\text{step}} = \sqrt{3} v_c / 100$. Results are presented in terms of the transient rate divided by the steady-state rate

$$\frac{J(t)}{J_{\text{SS}}} = \frac{f_G(t)}{f_G(\infty)}$$
$$= 1 + \frac{\beta_{v_{\text{step}}} \mathbf{D}^{-1/2}(G,G) \sum_j \langle \psi(0) | V_j \rangle \exp(-\lambda_j t)(V_j)_G}{J_{\text{SS}}}. \tag{4.21}$$

Further scaling is accomplished by defining the dimensionless time $\tilde{t} = \beta_{v_{\text{step}}} t$ and dividing concentrations by the concentration of smallest droplets $n_0 \approx n_0^0$. In these units, the elements **K**, for example, depend only on ε, which determines the population ratios appearing in Eqs. (4.4) or (4.10). The same holds for the reduced nucleation rate [left-hand side of Eq. (4.21)]. Original units are easily restored at the end of a calculation by multiplying scaled rates by $\beta_{v_{\text{step}}} n_0$. For the initial conditions we set the population of clusters to follow Eq. (4.1), which is the cloud droplet distribution in the absence of collection and there is no current. At $t = 0$ collection is turned on and the population evolves according to Eq. (4.19), and current according to Eq. (4.21).

Figure 7 shows the reduced transient rate $J(t)/J_{\text{SS}}$ in reduced time units for different values of ε. The calculations are described in Appendix B. Results from the full matrix calculations of Eq. (4.21) (solid curves in Fig. 7) are compared with those obtained using a simple lognormal parametrization provided in B (dashed curves). The parametrization gives excellent results for higher values of the barrier height and continues to work reasonably well throughout the activated regime. Unfortunately it is the important short time behavior for which the parametrization first has difficulty—beginning at about $\Phi^* \approx 5$ as the barrier height is reduced—forcing one to return to Eq. (4.21) if very accurate prediction of the early onset of drizzle formation is desired in this regime. Similar difficulties arise when the lognormal parametrization is used to approximate transient rates in nucleation theory [8].

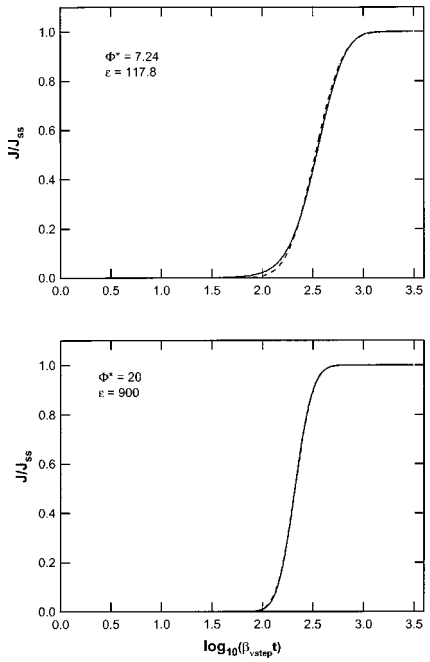

FIG. 7. Transient drizzle rate. Barrier crossing rate divided by the steady-state rate versus the logarithm of the reduced time. Solid curves: full matrix-eigenvalue calculation from Eq. (4.21). Dashed curves: lognormal parametrization of Eqs. (B8) and (B9).

From the results of Fig. 7 it is seen that the onset of drizzle formation will typically occur on time scales that are fractionally much shorter than those required to reach steady state. Thus, when drizzle occurs, it will likely be initiated under transient conditions. This is illustrated further in Fig. 8 which shows the conditions required to reach transient drizzle onset rates $J(t)$ of 10^{-5} to 10^{-6} cm^{-3} s^{-1}, or 1–10 drops per cubic meter of cloud per second. These are estimated rates required for significant drizzle formation assum-

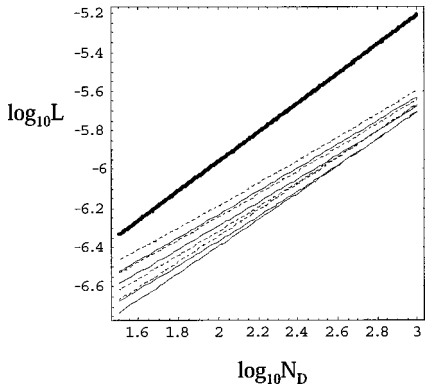

FIG. 8. Contours of constant transient drizzle formation rate, $J(t)$cm^{-3} s^{-1} for several drizzle waiting times (t) defined as the time since collection is turned on ($t = 0$). Solid curves: $\log_{10} J(t) = -6$; top to bottom: $t = -600$, 1200, 3600, infinity = steady state. Dashed curves: $\log_{10} J(t) = -5$; top to bottom: $t = 600$, 1200, 3600, infinity = steady state. Contours calculated using the parametrization Eqs (B8) and (B9) with Eq. (3.12) for the steady-state drizzle rate. Thick line, separation boundary between the kinetic and activated cloud regimes $\{\varepsilon = (3/2)^4\}$. Results are for $t_{1\%} = 0.1$ s.

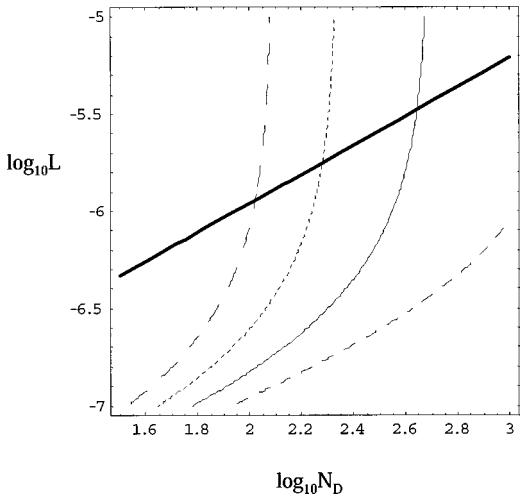

FIG. 9. Collection time. Time required in seconds for a post-critical drizzle embryo (of volume $v=\sqrt{3}v_c$, where v_c is the critical droplet volume) to reach 50 μm radius in size. Contours right to left $\{t_{50}=500,1000,1500,2000\}$ from Eq. (A11). Results are for $t_{1\%}=0.1$ s. This added to the drizzle formation (waiting) times from Fig. 8 gives the total time required to form a corresponding flux of 50 μm radius drops. Thick line, separation boundary between the kinetic and activate cloud regimes $\{\varepsilon=(3/2)^4\}$. Results are for $t_{1\%}=0.1$ s.

ing a radius of 100 μm for the collected droplets [5]. The figure shows the conditions required to obtain these rates within time periods of 10, 20 min, and 1 h following the turning on of collection in the model at $t=0$. The steady-state contours for $J(\infty)=10^{-5}$ and 10^{-6} cm^{-3} s^{-1} from Fig. 6 are also reproduced (lowest solid and lowest dashed curves in Fig. 8). It is seen that as the allowed onset time for observable drizzle formation is reduced, the contours shift towards larger values of ε; conditions that also favor a higher steady-state drizzle rate. In the limit of an infinite onset period, the transient contours coincide with those for the same rate at steady state. Figure 9 shows the collection time, defined here as the time required for a newly formed drizzle droplet to reach a radius of 50 μm, which is the largest size for which Eq. (2.4) applies [11]. The calculation is described in Appendix A. The collection time added to the drizzle formation time (Fig. 8) gives the total time required to form the corresponding flux of 50 μm drizzle drops.

V. SUMMARY AND DISCUSSION

A description of the onset of drizzle formation has been developed using kinetic potential theory. Drizzle is described quantitatively as an activated barrier crossing phenomenon using methods borrowed from homogeneous nucleation theory. Two types of calculations were presented: (1) matrix-eigenvalue calculations of the kinetics of steady-state and transient drizzle formation and (2) comparisons of these with results from simple analytic expressions and parametrizations valid in the all-important activated cloud regime. This ability to yield analytic expressions for the steady-state drizzle rate, activation barrier height, and critical droplet size is an especially attractive feature of the kinetic potential theory. More work remains to be done, especially in the post-drizzle-initiation regime, but the new methods should lead to improved parameterizations for aerosol-cloud interactions and subsequent improvements to weather forecast and climate models.

Modeling of the later stages of drizzle formation will require relaxing both of the nucleation boundary conditions employed in Secs. III and IV. Candidate approaches include method-of-moments type calculations in which lower-order moments of the combined cloud and drizzle droplet distributions are tracked in time; similar to the description of vapor depletion effects through the integrated treatment of nucleation and growth processes during gas to particle conversion [15]. Closure of the moment evolution equations can be obtained using quadrature methods developed for aerosol dynamics simulation [22]. Another approach, which would yield a sampled representation of the drizzle droplet spectrum, instead of moments, is to simply extend the range of the matrix calculations of Sec. IV using a sampling grid that extends beyond the Szilard boundary so as to include much larger droplet sizes. Both approaches are good candidates for future extensions of the present threshold model.

Of all of the cloud processes successfully integrated into the kinetic potential theory of drizzle formation, the role of turbulence remains the least understood. At its present stage of development, the model requires that the turbulence parameter $\beta^{\rm cond}$, the underlying cloud droplet distribution, and the collection rate constant κ each be prescribed. Accordingly the present model is incapable of addressing likely correlations between $\beta^{\rm cond}$ and the cloud droplet distribution, and between $\beta^{\rm cond}$ and κ. Once such correlations are understood and incorporated, the model should provide a much clearer understanding of how cloud turbulence fluctuations couple with drizzle formation.

The analysis of Sec. III has shown the possibility for two distinct regimes of drizzle formation: a kinetically-controlled regime and an activated regime. It is the activated regime of drizzle formation that is best supported by observations. These include (1) the negative correlation seen between cloud droplet concentration and drizzle rate and (2) the general observation, built into current state-of-the-art empirical parametrizations, that drizzle formation is a threshold phenomenon [4,18]. Because cloud droplets form on aerosol particles, the negative correlation between droplet concentration and drizzle rate is manifested through the well-known effect that aerosols have on drizzle suppression [7,2]. The present calculations are fully consistent with both observations in the activated regime while predicting very different behavior in the kinetic regime. This raises an interesting paradox for the model: how can the existence of a barrier to drizzle actually serve to promote drizzle formation? While a complete answer requires including effects from cloud droplet depletion during collection, considerable insight is available from results already obtained: The barrier regulates the rate at which cloud droplets can enter the collection regime. Out of the millions of cloud droplets present in a cubic meter of cloud, only $1-10$ (per s) are needed to provide an observable drizzle rate. The barrier simply serves to limit the rate at which collection-size droplets can form so that such small

frequencies of crossing events can be realized. Droplets that do manage through chance fluctuations to cross the barrier will experience rapid growth to fallout size before the effects of depletion set in. If instead the process was activationless, so that many drops of collection size could be initiated at the same time, the subsequent competition for cloud water would likely prevent any of them from reaching large size.

There is another property of depletion that will tend to favor drizzle formation in the activated regime: To first order the collection process depends on the size of the collecting drop but is independent of the smaller cloud droplet size [Eq. (2.4)]. Thus we might expect that during depletion, both N_D and L will be reduced at a proportional rate along the direction of the dashed contour lines of constant averge droplet volume shown in Fig. 6. A comparison of the slopes of the solid and dashed contours in Fig. 6 implies a threshold reduction in the drizzle rate with proportional depletion of N_D and L. Under these conditions, the depletion of cloud droplets through collection will exert an inhibitory feedback control that quenches drizzle formation in much the same way that vapor depletion quenches nucleation, often resulting in oscillatory rates of nucleation and growth [15]. While the full dynamics of the later stages of drizzle remain to be incorporated in the model, the preceding arguments suggest that depletion will act as a nonlinear feedback mechanism for keeping cloud conditions within the activated regime and close to or below the threshold for drizzle formation.

This paper has developed the kinetic potential theory and extended its range of application beyond its origins in nucleation theory to a system, drizzle formation, for which neither temperature nor thermodynamic potential are well defined. These advances will open the door to applications of the kinetic potential theory to other areas of statistical physics, applied mathematics, and perhaps economics, where phenomena that can be modeled as sequences of transition rates or transition probabilities arise.

ACKNOWLEDGMENTS

The authors thank Drs. Peter H. Daum and Stephen E. Schwartz of BNL for helpful discussions. This research was supported by the Environmental Sciences Division of the U.S. Department of Energy, as part of the Atmospheric Chemistry Program under Contract No. DE-AC02-76CH00016, the Atmospheric Radiation Measurements Program under Contract DE-AC03-98CH10886, and a LDRD grant from BNL.

APPENDIX A: FLUCTUATIONS AND GROWTH IN THE COLLECTION REGIME

From Eq. (2.10b),

$$\Phi(v) = \frac{\Phi^*}{2}\left[3\frac{v}{v_c} - \left(\frac{v}{v_c}\right)^3\right] = \frac{1}{3}\frac{v_c}{v}\left[3\frac{v}{v_c} - \left(\frac{v}{v_c}\right)^3\right] \quad \text{(A1)}$$

and

$$\frac{d\Phi}{dv} = \frac{1}{v}\left[1 - \left(\frac{v}{v_c}\right)^2\right]. \quad \text{(A2)}$$

This last result gives the gradient of the kinetic potential along the droplet volume coordinate. The gradient is proportional to force (but in the opposite direction) and should therefore be proportional to the velocity along the volume coordinate in a Brownian fluctuation model:

$$\frac{dv}{dt} = \eta F, \quad \text{(A3)}$$

where η is mobility. Long's collection kernel requires that in the collection limit the growth velocity be given by Eq. (2.4):

$$\frac{dv}{dt} = \kappa L v^2. \quad \text{(A4)}$$

It is interesting to explore the equivalence of Eqs. (A3) and (A4) and determine the mobility.

In the collection limit ($v \gg v_c$) Eq. (A2) is approximated as

$$\frac{d\Phi}{dv} \approx -\frac{1}{v}\left(\frac{v}{v_c}\right)^2 = -\frac{\kappa L}{\beta^{\mathrm{cond}} v_1^2} v^2, \quad \text{(A5)}$$

where the last equality follows substitution from Eq. (2.11b) for v_c^2. Together Eqs. (A4) and (A5) give a linear response relation between the potential gradient and the rate of growth

$$\frac{dv}{dt} = -\beta^{\mathrm{cond}} v_1^2 \frac{d\Phi}{dv} = -D_v \frac{d\Phi}{dv} = \kappa L v^2. \quad \text{(A6)}$$

This analysis shows consistency between the collection growth law, the shape of the kinetic potential in the collection regime, and the turbulence fluctuations in evaporation and growth embodied in the diffusion parameter D_v.

It is interesting to notice that Eq. (A6) has the form one would expect by analogy with thermodynamic fluctuation theory applied to systems which, unlike the drizzle model, have well defined temperature (T) and thermodynamic potential (W). To illustrate, let x denote a general coordinate and set $\Phi(x) = W(x)/kT$. The analogous relation to Eq. (A6) is

$$\frac{dx}{dt} = \eta F = -\eta \frac{dW(x)}{dx} = -\eta kT \frac{d\Phi(x)}{dx} = -D\frac{d\Phi(x)}{dx}. \quad \text{(A7)}$$

In the first equality F is force and η is mobility. The fourth equality is the well-known Einstein relation between diffusion and mobility [23]:

$$D = kT\eta. \quad \text{(A8)}$$

The preceding analysis shows that Eq. (A6) is consistent with the thermodynamic result despite the fact that in its derivation neither temperature nor thermodynamic potential have been defined. The preceding argument also demonstrates the validy of equating $\beta^{\mathrm{cond}} v_1^2$ with the diffusion coefficient D_v. Nevertheless an important difference remains: in the drizzle model fluctuations occur on the energy scale of turbulence—not kT.

The deterministic growth of freshly nucleated particles, once they cross the Szilard boundary at $v=\sqrt{3}v_c$, is described by Eq. (A2)

$$\frac{dv}{dt} = -D_v\frac{d\Phi}{dv} = -D_v\frac{1}{v}\left[1-\left(\frac{v}{v_c}\right)^2\right] = \kappa L v^2 - \frac{D_v}{v}. \tag{A9}$$

The last equality follows Eq. (A5). This is a first-order nonlinear differential equation of a fairly standard form whose solution is

$$v(t) = \frac{v_c}{\tanh(d-\kappa L v_c t)}. \tag{A10a}$$

The constant of integration is obtained from the initial condition, and is for particles beginning their growth at the Szilard boundary $v(0)=\sqrt{3}v_c$:

$$d = \tanh^{-1}(1/\sqrt{3}) \approx 0.658. \tag{A10b}$$

The time required for droplets to grow from the Szilard boundary to 50 μm radius [the limit of the collection kernel of Eq. (2.4)] is, accordingly,

$$t_{50} = \frac{d-\tanh^{-1}(v_c/v_{50})}{\kappa L v_c}, \tag{A11}$$

where v_{50} is the volume of a 50 μm radius drop. This added to the drizzle formation time gives the total time required to form a flux of 50 μm radius drops.

APPENDIX B: A PARAMETRIZATION FOR THE TRANSIENT BARRIER CROSSING RATE

As found in nucleation theory, the approach to steady state is described with good accura in terms of the temporal moments [8]:

$$M_k = \int_0^\infty t^k[1-J(t)/J_{ss}]dt = \frac{1}{k+1}\int_0^\infty t^{k+1}p(t)dt \equiv \frac{\mu_{k+1}}{k+1}, \tag{B1}$$

where $J(t)$ and J_{ss} are, respectively, the transient and steady-state drizzle rates and μ_k is the kth moment of $p(t)$:

$$p(t) = \frac{1}{J_{ss}}\frac{d}{dt}J(t). \tag{B2}$$

$M_0=\mu_1$ is the lag time for drizzle formation. The second equality of Eq. (B1) follows an integration by parts.

In the case of the nucleation time lag it has been found that a log-normal distribution can give a good approximation to $P(t)$ yielding a parametrization for $J(t)$ in terms of lowest-order moments [8]. A similar result is found for the drizzle rate provided the barrier height Φ^* is not too small. From Eqs. (B2), (4.8), and (4.21) we obtain

$$P(t) = -\frac{\sqrt{n_G}}{(g_{SS})_G}\sum_j \langle\psi(0)|V_j\rangle\lambda_j \exp(-\lambda_j t)(V_j)_G \tag{B3}$$

which on integration over t yields the moments

$$\mu_k = -\frac{\sqrt{n_G}}{(g_{SS})_G}k!\sum_j \langle\psi(0)|V_j\rangle\frac{1}{\lambda_j^k}(V_j)_G. \tag{B4}$$

Approximating $P(t)$ by the normalized log-normal distribution

$$f_{\mathrm{Ln}}(t) = (ts\sqrt{2\pi})^{-1}\exp[-(\ln t - m)^2/2s^2], \tag{B5}$$

which has the moments

$$\int_0^\infty t^k f_{\mathrm{Ln}}(t) = \exp[km + (ks)^2/2], \tag{B6}$$

enables the log-normal parameters m and s^2 to be expressed in terms of moments:

$$s^2 = \ln\left(\frac{\mu_2}{\mu_1^2}\right) = \ln\left(\frac{2M_1}{M_0}\right), \tag{B7a}$$

$$m = -\frac{1}{2}\ln\left(\frac{\mu_2}{\mu_1^4}\right) = -\frac{1}{2}\ln\left(\frac{2M_1}{M_0^4}\right). \tag{B7b}$$

In reduced time units $\tilde{t}=\beta_{v_{\mathrm{step}}}t$ the transient profile depends only on the non-dimensional parameter ε of Sec. III. This property enables a parameterization of the log-normal parameters solely in terms of ε. Calculations were carried out for the moments over the range of barrier height from 5–20 ($56\leqslant\varepsilon\leqslant900$) using the matrix method [Eq. (B4)]. From the moments we obtained s^2 and m from Eqs. (B7) and the fits

$$m(\varepsilon) = 5.80882 - 0.0583523\sqrt{\varepsilon} + 0.000451818\varepsilon + 0.296341\ln\left(\frac{2\sqrt{\varepsilon}}{3}\right), \tag{B8a}$$

$$s^2(\varepsilon) = 0.968544 + 0.0281779\sqrt{\varepsilon} - 0.000219704\varepsilon - 0.504727\ln\left(\frac{2\sqrt{\varepsilon}}{3}\right). \tag{B8b}$$

The transient rate behavior is given by Eq. (B2), with the log-normal approximation to $P(t)$, as the cumulative distribution

$$\frac{J(\tilde{t})}{J_{\mathrm{SS}}} \approx 1 - \frac{1}{2}\mathrm{erfc}\left[\frac{\ln(\tilde{t})-m}{\sqrt{2s^2}}\right], \tag{B9}$$

where erfc is the complementary error function. Values for m and s^2 are obtained for a specified, in-range value of ε from Eqs. (B8). Equation (B9) was used to obtain the normalized transient rate curves of Fig. 7, which are in very good agreement with the results of the full matrix eigenvalue calculation.

[1] M. B. Baker, Science **276**, 1072 (1997).
[2] D. Rosenfeld, Science **287**,1793 (2000).
[3] N. V. Gillani, P. H. Daum, S. E. Schwartz, W. R. Leaitch, J. W. Strapp, and G. A. Isaac, in *Preciptitation Scavenging and Atmopsheric Surface Exchange* edited by S. E. Schwartz and W. G. N. Slinn (Hemisphere, Washington, D.C., 1992), Vol. 1, pp. 359–369.
[4] E. Kessler, Meteorol. Monogr. **10**, 1 (1969).
[5] R. McGraw and Y. Liu, Phys. Rev. Lett. **90**, 018501 (2003).
[6] P. Squires, Tellus **10**, 256 (1958).
[7] B. A. Albrecht, Science **245**, 1227 (1989).
[8] D. T. Wu, Solid State Phys. **50**, 37 (1997).
[9] F. F. Abraham, *Homogeneous Nucleation Theory* (Academic, New York, 1974).
[10] P. G. Debenedetti and H. Reiss, J. Chem. Phys. **108**, 549 (1998).
[11] A. B. Long, J. Atmos. Sci. **31**, 1040 (1974).
[12] C. Kittel, *Elementary Statistical Physics* (Wiley, New York, 1958), pp. 175 and 176.
[13] R. McGraw, J. Phys. Chem. B **105**, 11838 (2001).
[14] S. Chandrasekhar, in *Selected Papers on Noise and Stochastic Processes*, edited by N. Wax (Dover, New York, 1954), pp. 5.
[15] R. McGraw and J. H. Saunders, Aerosol Sci. Technol. **3**, 367 (1984).
[16] D. W. Oxtoby and R. J. Evans, J. Chem. Phys. **89**, 7521 (1988).
[17] D. Reguera and H. Reiss (unpublished).
[18] Y. Liu and P. H. Daum, J. Atmos. Sci. **61**, 1539 (2004).
[19] Y. Liu, P. H. Daum, and R. McGraw, Geophys. Res. Lett. **31**, L06121 (2004).
[20] W. J. Shugard and H. J. Reiss, J. Chem. Phys. **65**, 2827 (1976).
[21] F. J. Schelling and H. Reiss, J. Chem. Phys. **74**, 3527 (1981).
[22] R. McGraw and D. L. Wright, J. Aerosol Sci. **34**, 189 (2003).
[23] J. P. Boon and S. Yip, *Molecular Hydrodynamics* (Dover, New York, 1991), p. 66.